JEM Journal of Experimental Medicine

BRIEF DEFINITIVE REPORT

CXCR4 regulates *Plasmodium* development in mouse and human hepatocytes

Hironori Bando[1], Ariel Pradipta[1], Shiroh Iwanaga[6,7], Toru Okamoto[2], Daisuke Okuzaki[4], Shun Tanaka[1,3], Joel Vega-Rodríguez[8], Youngae Lee[3], Ji Su Ma[1,3], Naoya Sakaguchi[1,3], Akira Soga[5], Shinya Fukumoto[5], Miwa Sasai[1,3], Yoshiharu Matsuura[2], Masao Yuda[7], Marcelo Jacobs-Lorena[8], and Masahiro Yamamoto[1,3]

The liver stage of the etiological agent of malaria, *Plasmodium*, is obligatory for successful infection of its various mammalian hosts. Differentiation of the rod-shaped sporozoites of *Plasmodium* into spherical exoerythrocytic forms (EEFs) via bulbous expansion is essential for parasite development in the liver. However, little is known about the host factors regulating the morphological transformation of *Plasmodium* sporozoites in this organ. Here, we show that sporozoite differentiation into EEFs in the liver involves protein kinase C ζ–mediated NF-κB activation, which robustly induces the expression of C-X-C chemokine receptor type 4 (CXCR4) in hepatocytes and subsequently elevates intracellular Ca^{2+} levels, thereby triggering sporozoite transformation into EEFs. Blocking CXCR4 expression by genetic or pharmacological intervention profoundly inhibited the liver-stage development of the *Plasmodium berghei* rodent malaria parasite and the human *Plasmodium falciparum* parasite. Collectively, our experiments show that CXCR4 is a key host factor for *Plasmodium* development in the liver, and CXCR4 warrants further investigation for malaria prophylaxis.

Introduction

The 2017 World Health Organization report estimates that nearly 440,000 deaths were caused by infection with the obligatory protozoan human malaria parasite, *Plasmodium*. Malaria, one of the most important vector-borne diseases, occurs when *Plasmodium* parasites are transmitted via *Anopheles* mosquitoes to mammalian hosts such as humans (Shortt and Garnham, 1948; Meis et al., 1983; Cowman et al., 2016). The life cycle of *Plasmodium* parasites is divided into three stages: the vector stage in the mosquito and the liver and blood stages in the host. During the vector stage, *Plasmodium* forms oocysts in the mosquito midgut from which the next life stage (sporozoites) moves to the salivary glands and acquires infectivity to mammalian hosts. Infection starts with the delivery of sporozoites to the host by the bite of a *Plasmodium*-infected mosquito. Sporozoites first enter the blood circulation and then the liver, where they invade hepatocytes (Prudêncio et al., 2006; Ménard et al., 2008). After this, they develop further as exoerythrocytic forms (EEFs; Shortt and Garnham, 1948; Hollingdale et al., 1983; Meis et al., 1983, 1985; Calvo-Calle et al., 1994). Each EEF generates the release of thousands of merozoites into the bloodstream, where they invade erythrocytes, initiating the blood stages of infection and causing clinical malarial disease (Prudêncio et al., 2006). Thus, the development of *Plasmodium* parasites in the liver is an obligatory stage for the successful infection of their mammalian hosts (Shortt and Garnham, 1948; Meis et al., 1983; Cowman et al., 2016).

After their arrival at the liver, sporozoites traverse the host cells such as Kupffer cells and hepatocytes and form parasitophorous vacuoles (PVs) in the finally invaded hepatocytes (Mota et al., 2001). Although the sporozoite traverse of dermis and Kupffer cells is indispensable for liver-stage development into EEFs in vivo (Amino et al., 2008; Tavares et al., 2013), the cell traversal itself is dispensable for liver-stage parasite development in vitro, since traverse-deficient parasites form normal liver-stage development in hepatocytes (Ishino et al., 2004, 2005) suggesting that sporozoite infection into hepatocytes,

[1]Department of Immunoparasitology, Osaka University, Osaka, Japan; [2]Department of Molecular Virology, Research Institute for Microbial Diseases, Osaka University, Osaka, Japan; [3]Laboratory of Immunoparasitology, World Premier International Immunology Frontier Research Center, Osaka University, Osaka, Japan; [4]Genome Information Research Center, Osaka University, Osaka, Japan; [5]National Research Center for Protozoan Diseases, Obihiro University of Agriculture and Veterinary Medicine, Obihiro, Japan; [6]Department of Environmental Parasitology, Graduate School of Medical and Dental Sciences, Tokyo Medical and Dental University, Tokyo, Japan; [7]Department of Medical Zoology, Mie University School of Medicine, Mie, Japan; [8]Department of Molecular Microbiology and Immunology, Johns Hopkins Bloomberg School of Public Health, Johns Hopkins Malaria Research Institute, Baltimore, MD.

Correspondence to Masahiro Yamamoto: myamamoto@biken.osaka-u.ac.jp; J. Vega-Rodríguez's present address is Laboratory of Malaria and Vector Research, National Institute of Allergy and Infectious Diseases, National Institutes of Health, Rockville, MD.

rather than the cell traverse, is important for liver-stage development. Sporozoites from the rodent malaria parasite *Plasmodium berghei* invade rodent hepatocytes, causing hepatocyte growth factor (HGF) secretion and activating the receptor tyrosine kinase MET, resulting in suppressed hepatocyte apoptosis and facilitating sporozoite development into EEFs (Leirião et al., 2005). Although the Leirião et al. (2005) study strongly suggested that the development of *P. berghei* in the liver involves host factors, activation of the HGF–MET signaling pathway is not essential for liver-stage *Plasmodium yoelii* rodent malaria parasites or the *Plasmodium falciparum* human malaria parasite (Kaushansky and Kappe, 2011). Thus, little is known about the common regulatory circuit that is active during liver-stage development in *Plasmodium* species.

In the mosquito vector, *Plasmodium* sporozoites are rod shaped. After invading hepatocytes, the rod-shaped sporozoites undergo bulbous expansion and transform into spherical EEFs (Hollingdale et al., 1983; Meis et al., 1985; Calvo-Calle et al., 1994). The morphological transformation of sporozoites into early EEFs can be induced outside of hepatocytes and is known to require serum and an optimal temperature of 37°C (Kaiser et al., 2003). Ca^{2+} is known to regulate temperature-dependent sporozoite development into EEFs under cell-free conditions (Doi et al., 2011). However, it is also known that ectopic morphological transformation of sporozoites outside hepatocytes is detrimental to the life cycle of *Plasmodium* parasites, as *P. berghei* lacking PUF2, an RNA-binding protein, displays spherical EEF-like parasites in the mosquito salivary glands, resulting in failure of parasite invasion into hepatocytes (Gomes-Santos et al., 2011). Thus, it seems likely that morphological transformation into EEFs may be tightly controlled so that it only occurs in hepatocytes during the parasite's life cycle; however, the host factors that critically regulate the morphological transformation of sporozoites, as well as their differentiation into EEFs in the infected hepatocytes, lack understanding.

Here, we sought to determine the host factors and molecular mechanisms involved in the *P. berghei* sporozoite morphological transformation into EEFs in hepatocytes. Our study identified C-X-C chemokine receptor type 4 (CXCR4) as the master developmental regulator of *P. berghei* and *P. falciparum* in hepatocytes.

Results and discussion

HGF-induced MET signaling in hepatocytes is required for *P. berghei* development

After hepatocyte invasion, *P. berghei* rod-shaped sporozoites start a bulbous expansion and transform into spherical EEFs (Fig. 1 A; Shortt and Garnham, 1948; Meis et al., 1983, 1985). We sought to identify the host hepatocyte–derived factors that are required for transformation of the rod-shaped sporozoites into spherical EEFs. As previously reported (Carrolo et al., 2003), we confirmed that HGF is required for the formation of EEFs using a *P. berghei*–human hepatoma Huh7 cell-line system (Fig. 1 B). Treatment with anti-HGF antibodies did not affect the invasion rates (Fig. S1, A and B; Mueller et al., 2005b). Moreover, anti-HGF treatment resulted in reduced luciferase activation when constitutively luciferase-expressing *P. berghei* sporozoites were used to infect Huh7 cells (Figs. 1 C and S1 C). To test whether HGF is involved in sporozoite transformation, we examined the shapes of the parasites that successfully invaded the hepatocytes. While the distribution of the parasite shape was comparable in anti-HGF–treated or untreated Huh7 cells at 3 h after infection, the percentage of spherical parasites was significantly lower in the anti-HGF–treated Huh7 cells than those in the untreated cells at 24 h after infection (Fig. 1 D). Because HGF is the ligand for the tyrosine kinase MET receptor (Naldini et al., 1991), we next analyzed the role of MET using the MET-deficient (MET-KO) Huh7 cells we generated by CRISPR/Cas9 genome editing (Fig. S1 D). The resultant MET-KO Huh7 cells did not show growth factor–induced phosphorylation of AKT and ERK or degradation of IκBα, suggesting they were unresponsive to HGF stimulation (Fig. 1 E). We next tested *P. berghei* sporozoite transformation in MET-KO Huh7 cells (Fig. 1 F). Although the sporozoite invasion rate into MET-KO Huh7 cells and the parasite shape at 3 h after infection were comparable to those of WT cells (Figs. 1 F and S1 E), the percentage of spherical parasites in MET-KO cells at 24 h after infection was significantly lower than that in WT cells (Fig. 1 F). Furthermore, the parasite-derived luciferase activity at 48 h after infection in MET-KO cells was also severely reduced in comparison to that in WT cells (Fig. 1 G). Moreover, reconstituting MET expression in the MET-KO cells rescued the parasite-derived luciferase activity (Fig. S1, F and G), which excludes the possibility of off-target effects from the genome editing of the MET-KO cells. Taken together, these results demonstrate that HGF and the MET receptor are required for *P. berghei* sporozoite differentiation within hepatocytes, but not for parasite invasion.

Protein kinase C ζ (PKCζ) is required for *P. berghei* development in the liver

PKCζ has been shown to be involved in HGF signaling and NF-κB activation (Diaz-Meco and Moscat, 2012; Huang et al., 2012). When we investigated HGF-induced activation of AKT, ERK, and NF-κB in CRIPSR/Cas9 genome-edited PKCζ-KO Huh7 cells (Fig. S1 H), we found that phosphorylation of AKT and degradation of IκBα were completely absent, whereas phosphorylation of ERK was unaffected (Fig. 1 E). These results point to a bifurcation of HGF–MET signaling into ERK- and PKCζ-dependent signaling pathways. PKCζ has previously been shown to be involved in *P. berghei* sporozoite invasion of hepatocytes (Prudêncio et al., 2008). By contrast, we found that *P. berghei* sporozoite invasion of the PKCζ-KO Huh7 cells occurred normally (Fig. S1 I). The discrepancy might be related to the different methods used to assess parasite invasion (e.g., counting GFP-positive parasites relative to the total number host cells vs. counting UIS3-positive YFP-positive parasites relative to the total number of host cells) or to inhibited PKCζ (myristoylated PKCζ peptide vs. genome editing; Prudêncio et al., 2008). We next compared parasite-derived luciferase activity and parasite shape in WT and PKCζ-KO cells infected with *P. berghei* sporozoites (Fig. 1, H and I). Similar to MET-KO cells and anti-HGF–treated WT cells, spherical parasite formation was found to decrease in PKCζ-KO cells at 24 h after infection relative to WT cells (Fig. 1 H).

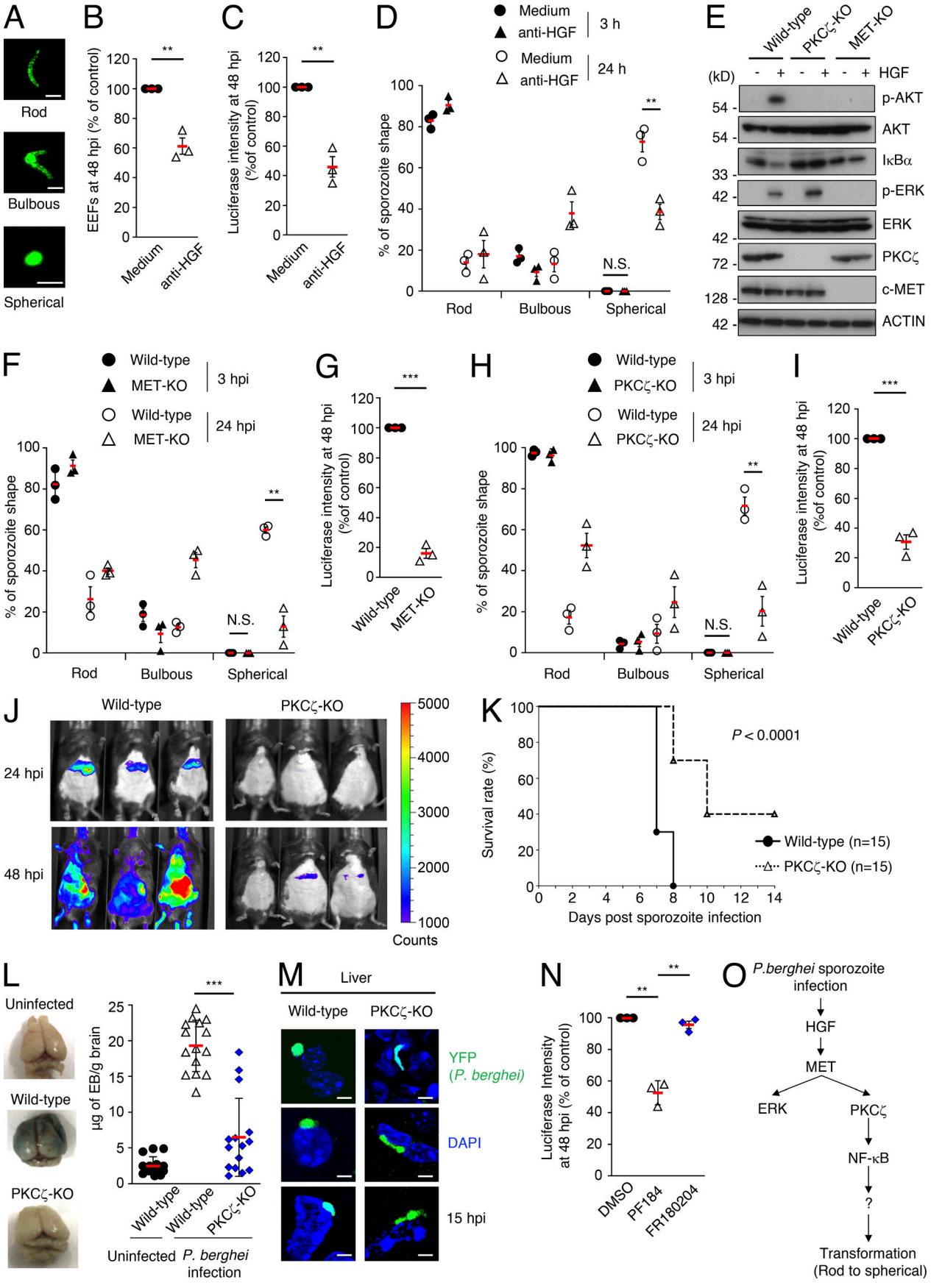

Figure 1. **The HGF–MET–PKCζ–NF-κB signaling pathway is required for liver-stage *P. berghei* development. (A)** Images illustrating sporozoite differentiation into EEFs in Huh7 cells. Rod-shaped sporozoites initially acquire a bulbous shape and subsequently become spherical. Bars, 5 µm. **(B–D)** Effect of addition of anti-HGF (20 µg/ml) antibody to the culture medium on *P. berghei* sporozoite development in Huh7 cells. **(B)** EEFs were counted using IFA. Indicated values are means (n = 3) ± SEM. Each point represents the mean of one experiment. Three experiments were repeated. **, P < 0.01 (Student's t test). **(C)** Luciferase intensity 48 h after sporozoite infection. Indicated values are means (n = 3) ± SEM. Each point represents the mean of one experiment. Three experiments were repeated. **, P < 0.01 (Student's t test). **(D)** Parasite shapes were assessed by IFA at the times after sporozoite infection indicated at the graphs. Indicated values are means (n = 3) ± SEM. Each point represents the mean of one experiment. Three experiments were repeated. **, P < 0.01 (Student's t test). **(E)** WT, PKCζ-KO, or MET-KO Huh7 cells were treated with 50 ng/ml HGF for 1 min. Expression of the genes indicated to the right was detected in the cell lysates by Western blotting. Numbers (in kilodaltons) to the left indicate the position of size markers. Data are representative of three independent experiments. **(F and G)** WT or MET-KO Huh7 cells were infected with *P. berghei* sporozoites. **(F)** Parasite shapes were assessed by IFA at the times after sporozoite infection indicated at the graphs. Indicated values are means (n = 3) ± SEM. Each point represents the mean of one experiment. Three experiments were repeated. **, P < 0.01 (Student's t test). **(G)** Luciferase intensity 48 h after sporozoite infection. Indicated values are means (n = 3) ± SEM. Each point represents the mean of one experiment. Three experiments were repeated. ***, P < 0.001 (Student's t test). **(H and I)** WT or PKCζ-KO Huh7 cells were infected with *P. berghei* sporozoites. **(H)** Luciferase intensity 48 h after sporozoite infection. Indicated values are means (n = 3) ± SEM. Each point represents the mean of one experiment. Three experiments were repeated. **, P < 0.01 (Student's t test). **(I)** Parasite shapes were assessed by IFA at the times after sporozoite infection indicated at the graphs. Indicated values are means (n = 3) ± SEM. Each point represents the mean of one experiment. Three experiments were repeated. ***, P < 0.001 (Student's t test). **(J–L)** WT mice (n = 15) or PKCζ-KO mice (n = 15) were infected with *P. berghei* sporozoites. **(J)** The progression of infection 24 or 48 h after sporozoite infection was measured using an in vivo imaging system. Data are representative of three independent experiments. **(K)** The survival rate was analyzed. Data are cumulative of three independent experiments. P < 0.0001 (log-rank test). **(L)** Blood–brain barrier integrity was measured by Evans Blue (EB) perfusion. Uninfected mice (n = 15) were used as controls. Data are cumulative of three independent experiments. Indicated values are means (n = 15) of ± SD. Each point represents the value of each mouse. **, P < 0.01 (Student's t test). **(M)** IFA image of WT or PKCζ-KO mice liver at 15 h after sporozoite infection. Bars, 5 µm. Images are three representatives out of five independent sections. **(N)** Effect of the addition of IKKβ inhibitor PF184 (500 nM) or ERK inhibitor FR180204 (10 µM) to the culture medium on *P. berghei* sporozoite development in Huh7 cells. Luciferase intensity 48 h after sporozoite infection is shown. Indicated values are means (n = 3) ± SEM. Each point represents the mean of one experiment. Three experiments were repeated. **, P < 0.01 (Student's t test). **(O)** Model of host signaling pathway for transformation of *P. berghei* sporozoite. N.S., not significant; hpi, hours post-infection.

Furthermore, PKCζ-KO Huh7 cells exhibited dramatically reduced parasite-derived luciferase activation at 48 h after infection (Fig. 1 I). The ectopic expression of PKCζ in PKCζ-KO cells was able to reconstitute the parasite-derived luciferase activity (Fig. S1, J and K). Because mice deficient in HGF or MET display an embryonically lethal phenotype (Bladt et al., 1995; Schmidt et al., 1995; Uehara et al., 1995), the physiological functions of HGF or MET cannot be tested in vivo. In contrast, PKCζ-KO mice are viable and healthy (Lee et al., 2013). Hence, we analyzed the physiological role of PKCζ in *P. berghei* sporozoite infections in vivo (Fig. 1, J–L; and Fig. S1, L–S). PKCζ-KO primary hepatocytes have defective activation of Akt and NF-κB in response to HGF stimulation (Fig. S1 N). When WT and PKCζ-KO mice were intravenously challenged with *P. berghei* sporozoites, the PKCζ-KO mice exhibited a delayed appearance of hepatic parasite-derived luciferase signals due to impaired liver-stage development and a lack of merozoites in reticulocytes (Figs. 1 J and S1 O), reduced parasitemia (Fig. S1 P), higher survival rates (Fig. 1 K), significantly reduced brain–blood barrier disruption (Fig. 1 L), and impaired sporozoite transformation into spherical forms in their livers (Fig. 1 M). In contrast, when PKCζ-KO mice were challenged with *P. berghei* merozoite-containing RBCs, they succumbed to parasitemia in a manner similar to that seen in WT mice (Fig. S1, Q and R). PKCζ plays a key role in T cell function (Martin et al., 2005). To exclude the possibility that PKCζ deficiency leads to resistance to *P. berghei* sporozoite infection, we transferred WT T cells into PKCζ-KO mice and assessed whether the sporozoite challenge recovers the susceptibility (Fig. S1 S). PKCζ-KO mice receiving WT T cells still exhibited resistance to the sporozoite challenge in a manner comparable to those receiving PKCζ-KO T cells (Fig. S1 S), indicating that loss of PKCζ in T cells may not determine the resistance in PKCζ-KO mice. Moreover, pharmacological blockade of NF-κB activation reduced the parasite-derived luciferase counts, whereas blockade of ERK activation did not (Fig. 1 N). Collectively, these data indicate that the HGF–MET–PKCζ–NF-κB signaling pathway is required for *P. berghei* sporozoite liver-stage development (Fig. 1 O).

CXCR4 is essential for *P. berghei* development in the liver

To explore the molecular mechanisms by which the HGF–MET–PKCζ–NF-κB pathway regulates *P. berghei* sporozoite development in hepatocytes (Fig. 1 O), we compared the gene expression patterns in WT and PKCζ-KO Huh7 cells treated or not treated with HGF. We also analyzed the gene expression profiles in WT and PKCζ-KO Huh7 cells uninfected or infected with *P. berghei* sporozoites (Figs. 2 A and S2 A). To exclude the host genes that are inducible by mosquito salivary gland extracts (mosquito debris), the gene expression profiles in mosquito debris–treated or untreated WT Huh7 cells were also analyzed (Figs. 2 A and S2 A). Among the 23,284 genes we analyzed by RNA sequencing (RNA-seq), 26 were PKCζ-dependent genes upregulated by both HGF stimulation and sporozoite infection, but not by mosquito debris alone (Figs. 2 A and S2 A). Next, the highly HGF-inducible genes were disrupted in the Huh7 cells by CRISPR/Cas9 genome editing, and protein expression was examined using Western blotting (Figs. 2 A and S2 B). Accumulation of certain proteins was significantly reduced in the genome-edited Huh7 cells, including CXCR4, sulfatase 2 (SULF2), zinc-finger protein 426 (ZNF426), and CD160, while other proteins such as chromosome 1 open reading frame 114 (C1orf114), C1 and TNF-related 4 (C1QTNF4), and nerve growth factor receptor (NGFR) were not (Fig. S2 B); this result is probably related to ineffective genome editing or has occurred by unknown reasons. Therefore, we selected the genome-edited cells where the levels of CXCR4, SULF2, ZNF426, and CD160

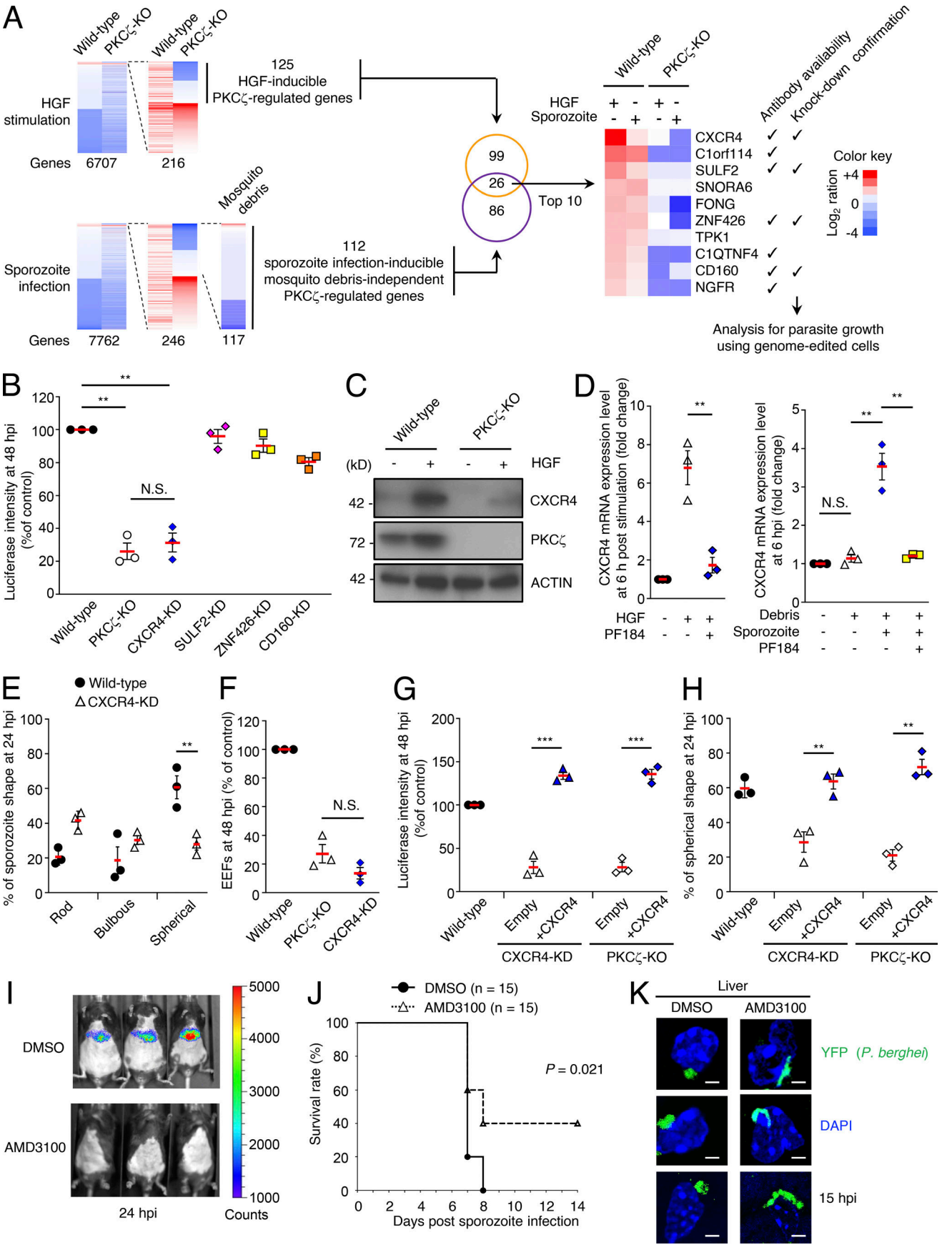

Figure 2. **CXCR4 is necessary and sufficient for liver-stage *P. berghei* development. (A)** Selection of PKCζ-dependent genes in 2.5 × 10^5 WT or PKCζ-KO Huh7 cells treated with HGF (50 ng/ml) or mosquito debris or infected with 5 × 10^5 *P. berghei* sporozoites for 6 h. Among 26 genes shared with both conditions (fully described in Fig. S2 A and the legend), the top 10 genes with indicated names are shown. Among the 10 genes, the expression of 7 genes could be assessed using commercially available antibodies ("Antibody availability"). Among these 7 genes, we confirmed that Huh7 cells with the genome editing of 4 genes showed reduction of the corresponding proteins ("Knock-down confirmation"; Fig. S2 B). The Huh7 cells with successful reduction of the indicated proteins were further tested for EEF formation assay in Fig. 2 B. Expression values are scaled up to the rows and range from −4 to +4. Data are from one experiment. **(B)** WT, PKCζ-KO, CXCR4-KD, SULF2-KD, ZNF426-KD, or CD160-KD Huh7 cells were infected with *P. berghei* sporozoites. Luciferase intensity was measured at 48 h after sporozoite infection. Indicated values are means (n = 3) ± SEM. Each point represents the mean of one experiment. Three experiments were repeated. **, P < 0.01 (Student's t test). **(C)** WT or PKCζ-KO Huh7 cells were treated or not with 50 ng/ml HGF for 24 h. The expression in the cell lysates of the genes indicated to the right was assessed by Western blotting. Numbers (in kilodaltons) to the left indicate the position of size markers. Data are representative of three independent experiments. **(D)** Huh7 cells were treated or not with PF184 (500 nM) or FR180204 (10 µM) for 4 h, as indicated. Also, cells were treated or not with 50 ng/ml HGF for 6 h and infected or not with sporozoites or treated with mosquito debris for 6 h, as indicated. The graphs report the quantitative RT-PCR analysis of CXCR4 mRNA levels. Indicated values are means (n = 3) ± SEM. Each point represents the mean of one experiment. Three experiments were repeated. **, P < 0.01 (Student's t test). **(E)** WT or CXCR4-KD Huh7 cells were infected with *P. berghei* sporozoites. Parasite shapes were assessed by IFA at 24 h after sporozoite infection. Indicated values are means (n = 3) ± SEM. Each point represents the mean of one experiment. Three experiments were repeated. **, P < 0.01 (Student's t test). **(F)** WT, PKCζ-KO, or CXCR4-KD Huh7 cells were infected with *P. berghei* sporozoites. EEFs at 48 h after sporozoite infection were counted using IFA. Indicated values are means (n = 3) ± SEM. Each point represents the mean of one experiment. Three experiments were repeated (Student's t test). **(G and H)** WT, CXCR4-KD, or PKCζ-KO Huh7 cells that were transfected with an empty vector (Empty) or with a vector expressing CXCR4 (+CXCR4) were infected with *P. berghei* sporozoites. **(G)** Luciferase intensity at 48 h after sporozoite infection. Indicated values are means (n = 3) ± SEM. Each point represents the mean of one experiment. Three experiments were repeated. ***, P < 0.001 (Student's t test). **(H)** Parasite shapes at 24 h after sporozoite infection were assessed by IFA. Indicated values are means (n = 3) ± SEM. Each point represents the mean of one experiment. Three experiments were repeated. **, P < 0.01 (Student's t test). **(I and J)** Mice untreated or treated with the CXCR4 inhibitor AMD3100 (10 mg/kg) were infected with *P. berghei* sporozoites. **(I)** The progression of infection 24 h after sporozoite challenge was measured using an in vivo imaging system. Data are representative of three independent experiments. **(J)** Comparison of survival rate. Data are cumulative of three independent experiments. P = 0.021 (log-rank test). **(K)** IFA image of DMSO- or AMD3100-treated mice liver 15 h after sporozoite infection. Bars, 5 µm. Images are three representatives out of five independent sections. N.S., not significant; hpi, hours post-infection.

were successfully reduced during sporozoite infection with *P. berghei*. Notably, we found severely decreased parasite-derived luciferase intensity in the Huh7 cells with reduced CXCR4 proteins in a manner similar to PKCζ KO cells, albeit with parasite invasion unaffected (Figs. 2 B and S3 A). On the other hand, Huh7 cells with reduction in the other proteins levels were unaffected (Fig. 2 B). Although the unstimulated WT Huh7 cells marginally expressed CXCR4, HGF stimulation strongly induced CXCR4 mRNA and protein expression in WT cells, but not in PKCζ-KO cells (Figs. 2 C and S3 B), in agreement with the RNA-seq analysis (Fig. 2 A). Furthermore, sporozoite infection of the Huh7 cells led to CXCR4 mRNA induction, and this was dependent on PKCζ and NF-κB but independent of mosquito debris (Figs. 2 D and S3 C). This suggests that the HGF–MET–PKCζ–NF-κB signaling pathway is important for CXCR4 up-regulation in response to sporozoite infection. We attempted to isolate the Huh7 cells lacking CXCR4 by limiting dilution but failed (data not shown), which may be related to the early embryonic lethality of the CXCR4-KO mice (Tachibana et al., 1998). Therefore, we used Huh7 cells with reduced CXCR4 protein expression levels (hereafter called CXCR4-knockdown [KD] Huh7 cells) for further investigation. The percentage of spherical parasites in the CXCR4-KD cells at 24 h after infection was significantly lower than that of WT cells, whereas the percentage was comparable to that of WT cells at 3 h (Figs. 2 E and S3 D). Compared with WT cells, CXCR4-KD cells showed reduced EEF formation, similar to PKCζ-KO cells (Fig. 2 F). Moreover, stable CXCR4 expression in CXCR4-KD cells fully rescued the development and transformation of the parasite (Fig. 2, G and H; and Fig. S3 E). Notably, ectopic expression of CXCR4 in PKCζ-KO Huh7 cells also rescued parasite infection and transformation (Fig. 2, G and H; and Fig. S3 F), indicating that CXCR4 expression downstream of the HGF–PKCζ–NF-κB signaling pathway is sufficient for *P. berghei* sporozoite development.

To test the role of CXCR4 in vivo, we used AMD3100, a potent CXCR4 inhibitor originally identified as an HIV entry blocker (Donzella et al., 1998) that is widely used in hematopoietic stem cell transplantation to treat patients with hematopoietic cancer (Giralt et al., 2014). After adding the *P. berghei* sporozoites onto a monolayer of WT Huh7 cells, AMD3100 treatment was found to reduce parasite development and transformation into the spherical forms (Fig. S3, G and H), which is reminiscent of the defective *P. berghei* transformation seen in PKCζ-KO and CXCR4-KD cells (Figs. 1 I and 2 E). We also challenged mice with *P. berghei* sporozoites in the presence or absence of AMD3100 pretreatment (Figs. 2, I and J; and Fig. S3, I and J). A delayed appearance of hepatic parasites and merozoites in reticulocytes was apparent in the AMD3100-pretreated mice (Figs. 2 I and S3 I). They also showed reduced parasitemia (Fig. S3 J), significantly higher survival rates (Fig. 2 J), and impaired sporozoite transformation into the spherical form in the livers of mice in comparison with control mice (Fig. 2 K). However, AMD3100 pretreatment did not affect the survival and parasitemia profiles of mice after infection with *P. berghei* merozoites (Fig. S3 K). Taken together, these results show that CXCR4 is necessary and sufficient for *P. berghei* liver-stage development downstream of the HGF–MET–PKCζ–NF-κB pathway.

CXCR4-induced Ca^{2+} regulates *P. berghei* development in hepatocytes

Next, we analyzed the mechanism underlying CXCR4 involvement in parasite development in mouse hepatocytes. CXCR4 is a well-known G protein–coupled receptor that elevates intracellular Ca^{2+} levels upon activation by its ligand (Littman, 1998;

Mellado et al., 2001). We observed HGF-induced intracellular Ca^{2+} increases in WT Huh7 cells (Fig. 3, A and B). In sharp contrast, PKCζ-KO and CXCR4-KD Huh7 cells did not show such an effect in response to HGF treatment (Fig. 3, A and B), which is consistent with PKCζ-dependent up-regulation of CXCR4 in response to HGF treatment (Fig. 2, A and C). Thus, PKCζ and CXCR4 are essential for the observed HGF-mediated Ca^{2+} increase in hepatocytes. We then hypothesized that the Ca^{2+} increase might be linked with sporozoite differentiation into EEFs, because Ca^{2+} has been reported to be involved in EEF development in the absence of host cells (Doi et al., 2011; Brochet and Billker, 2016). Serum and temperature (37°C) are both important factors for sporozoite transformation into early EEFs under cell-free conditions (Kaiser et al., 2003). Therefore, to confirm the role of Ca^{2+} in sporozoite development, we suspended *P. berghei* sporozoites in serum- and Ca^{2+}-free medium and conducted the assay in the presence or absence of Ca^{2+}. Although most of the sporozoites in the Ca^{2+}- and serum-free medium remained rod shaped and did not become spherical even after 24 h at 37°C, it is noteworthy that almost 40% of the sporozoites became spherical in Ca^{2+}-containing serum-free medium (Fig. 3 C). Furthermore, the host cell–free sporozoites in the Ca^{2+}-containing media lost the expression of sporozoite-specific (S-type) ribosomal RNA (rRNA) but possessed HSP70 protein (Fig. 3, D and E), which is expressed highly in early EEFs but barely in sporozoites (Kumar et al., 1993; Tsuji et al., 1994). Thus, our results also confirm that calcium regulates sporozoite development into early EEFs. Consequently, we examined whether CXCR4 is involved in sporozoite infection–induced elevation of intracellular Ca^{2+} levels in hepatocytes (Fig. 3 F). Strikingly, intracellular Ca^{2+} levels in *P. berghei* sporozoite-infected WT Huh7 cells were found to increase, unlike those in infected PKCζ-KO and CXCR4-KD cells and anti-HGF– and AMD3100-treated WT cells (Fig. 3 F).

Subsequently, PKCζ-KO and CXCR4-KD Huh7 cells or anti-HGF– and AMD3100-treated WT Huh7 cells were individually treated with ionomycin to forcibly elevate intracellular Ca^{2+} levels and parasite development, and transformation into spherical parasites was assessed (Fig. 3, G and H). Notably, ionomycin treatment restored parasite-derived luciferase activity (Fig. 3 G) and increased the rates of spherical parasites in PKCζ-KO or CXCR4-KD Huh7 cells and anti-HGF– and AMD3100-treated WT Huh7 cells (Fig. 3 H). Furthermore, the spherical parasites in PKCζ-KO and CXCR4-KD Huh7 cells or in anti-HGF– and AMD3100-treated WT Huh7 cells in response to ionomycin treatment were phenotypically judged to be EEFs, because the parasites expressed UIS4 on their PVs (Fig. 3 I), which is specifically expressed during the liver stage of *Plasmodium* development and is widely used as a marker of EEFs (Mueller et al., 2005a; Silva et al., 2016). When UIS4 expression was analyzed together with UIS3, which is expressed on the PV membrane and is a marker of PV formation (Mikolajczak et al., 2007), WT Huh7 cells were found to contain *P. berghei* parasites costained with anti-UIS3 and anti-UIS4 antibodies at 24 h after sporozoite infection (Fig. 3 J). In distinct contrast, PKCζ-KO and CXCR4-KD Huh7 cells or anti-HGF– and AMD3100-treated WT cells possessed parasites stained with anti-UIS3, but not (or barely) with anti-UIS4 (Fig. 3 J). Collectively, these results indicate that CXCR4-mediated intracellular Ca^{2+} increases trigger *P. berghei* sporozoite transformation into EEFs in hepatocytes.

CXCR4 regulates *P. falciparum* development in human hepatocytes

Because *P. berghei* is a murine parasite, we examined whether the important human pathogen *P. falciparum* also requires CXCR4 for its liver-stage development. *P. falciparum* sporozoites were found to transform into EEFs in the human hepatoma HC-04 cell line, but not in Huh7 cells (Fig. 4 A; Sattabongkot et al., 2006). Anti-HGF treatment of HC-04 cells did not affect *P. falciparum* EEF formation (Fig. S3 L), which is consistent with a previous finding that HC-04 cells infected with *P. falciparum* sporozoites do not activate HGF–MET signaling (Kaushansky and Kappe, 2011). We generated CXCR4-KD and PKCζ-KO HC-04 cells by CRISPR/Cas9 genome editing (Fig. S3 M) and examined the development and transformation of the parasites into spherical forms (Fig. 4, B–E). By counting circum sporozoite protein (CSP)–negative and RFP-positive parasites (Fig. 4 B), we found that invasion of *P. falciparum* sporozoites was comparable in WT, PKCζ-KO, and CXCR4-KD HC-04 cells (Fig. S3 N). Surprisingly, rates of spherical parasites at 24 h after sporozoite infection in CXCR4-KD or PKCζ-KO cells were lower than in WT cells (Fig. 4, B and C). Moreover, the size and number of EEF parasites at 7 d after *P. falciparum* sporozoite infection of CXCR4-KD or PKCζ-KO cell monolayers were smaller and significantly lower than in WT cells, respectively (Fig. 4, D and E). Next, we assessed the involvement of NF-κB and PKCζ in CXCR4 expression during *P. falciparum* sporozoite infections in vitro (Fig. 4, F and G). Although the NF-κB p65/RelA protein was cytoplasmically located in the uninfected HC-04 cells, nuclear translocation of p65/RelA was observed in *P. falciparum* sporozoite–infected cells (Fig. 4 F). In addition, although *P. falciparum* sporozoite–infected WT HC-04 cells showed markedly induced CXCR4 and CXCL12 mRNA levels, neither PKCζ-KO cells nor NF-κB inhibitor (PF184)– or mosquito debris–treated WT cells showed this effect (Figs. 4 G and S3 O). Moreover, blockage of CXCR4 by AMD3100 in WT HC-04 cells severely decreased the EEF numbers and resulted in impaired *P. falciparum* sporozoite transformation into spherical-form parasites (Fig. 4, H and I), whereas parasite invasion was not affected by the presence of AMD3100 (Fig. S3 P). Furthermore, the number of EEFs in AMD3100-treated primary human hepatocytes infected with *P. falciparum* sporozoites was reduced significantly (Fig. 4 J). Taken together, although HGF–MET signaling is dispensable (Kaushansky and Kappe, 2011), these results strongly indicate that CXCR4 and PKCζ are involved in the liver-stage development of *P. falciparum*.

In conclusion, we have identified CXCR4 as a host factor for the life cycle of liver-stage *P. berghei* and *P. falciparum* parasites. Activation of PKCζ signaling by HGF in *P. berghei* sporozoites, or by an unidentified event in the case of *P. falciparum* sporozoites, results in the induction of CXCR4 and a subsequent increase in intracellular Ca^{2+}, which in turn triggers differentiation of sporozoites into EEFs (Fig. 4 K). CXCR4-inhibited mice or PKCζ-KO mice are not completely resistant to sporozoite infection.

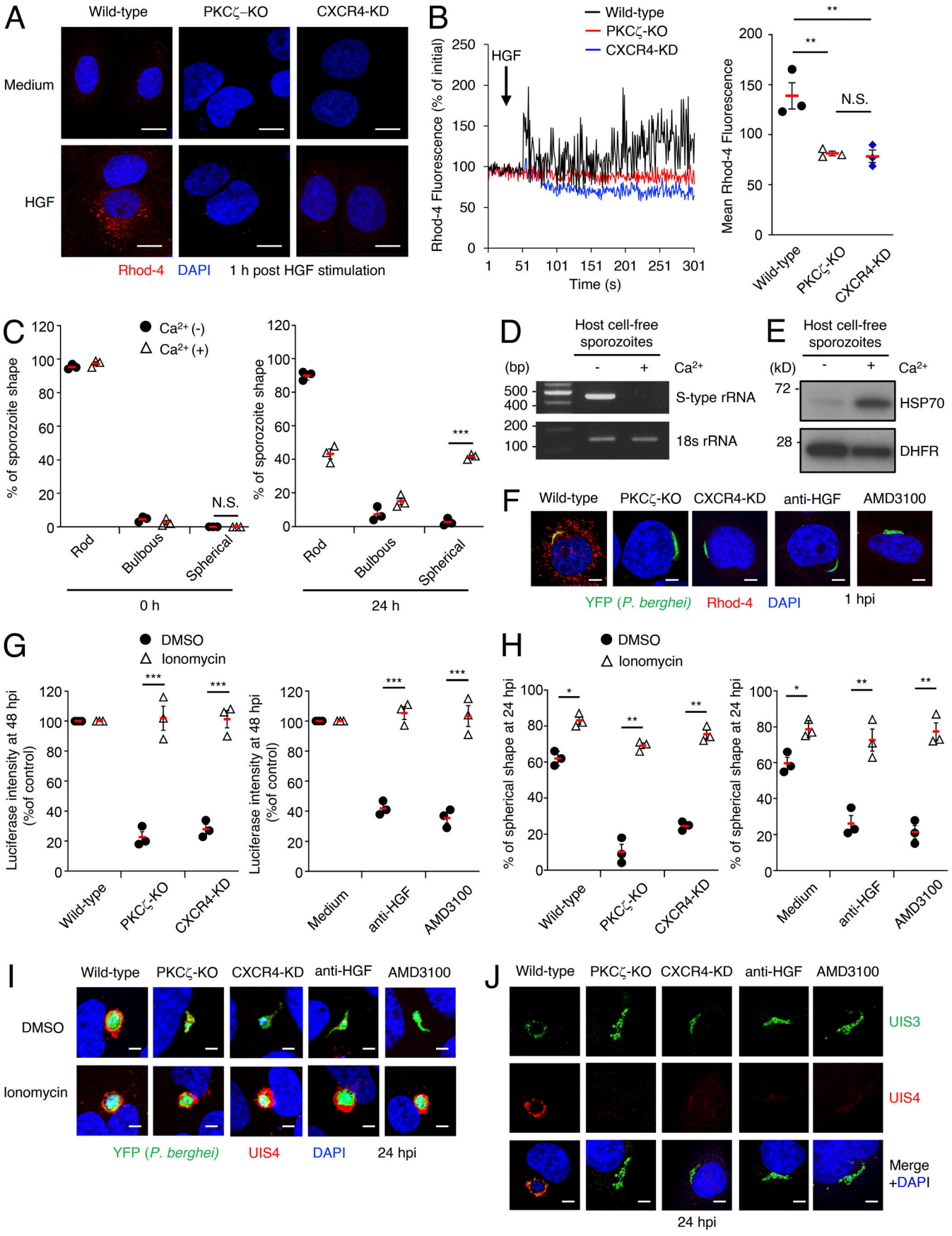

Figure 3. **CXCR4-mediated intracellular Ca^{2+} increase in hepatocytes triggers *P. berghei* sporozoite differentiation into EEFs. (A and B)** WT, PKCζ-KO, or CXCR4-KD Huh7 cells were stained with Rhod-4 (red) and DAPI (blue) and then treated or not with 50 ng/ml HGF for 1 h. **(A)** Representative images of the cells. Bars, 5 µm. Data are representative of three independent experiments. **(B)** Analysis of calcium flux in indicated cells. Indicated values are means (n = 3) ± SEM. Each point represents the mean of one experiment. Three experiments were repeated. **, P < 0.01 (Student's t test). **(C–E)** Effect of the addition of Ca^{2+} (1 mM) to the culture medium on host cell–free *P. berghei* sporozoite development. **(C)** Parasite shapes at 0 or 24 h after sporozoite infection were assessed by IFA. Indicated values are means (n = 3) ± SEM. Each point represents the mean of one experiment. Three experiments were repeated. ***, P < 0.001 (Student's t test). **(D)** RT-PCR analysis of S-type rRNA or 18s rRNA level in sporozoites. Data are representative of three independent experiments. **(E)** Expression of the genes indicated to the right was detected in the parasite lysates by Western blotting. Data are representative of three independent experiments. **(F)** WT, PKCζ-KO, CXCR4-KD, anti-HGF (20 µg/ml), or AMD3100 (1 µM) pretreated Huh7 cells were treated with Rhod-4 and then infected with *P. berghei* sporozoites for 1 h. Representative IFA images of the sporozoites in cells stained with YFP (green), DAPI (blue), and Rhod-4 (red). Bars, 5 µm. Data are representative of three independent experiments. **(G–J)** WT, PKCζ-KO, CXCR4-KD, anti-HGF (20 µg/ml), or AMD3100 (1 µM) pretreated Huh7 cells were treated or not with ionomycin (1 µg/ml) for 15 min, and cells were washed. Then cells were infected with *P. berghei* sporozoites. **(G)** Luciferase intensity at 48 h after sporozoite infection. Indicated values are means (n = 3) ± SEM. Each point represents the mean of one experiment. Three experiments were repeated. ***, P < 0.001 (Student's t test). **(H)** Parasite shapes 24 h after sporozoite infection were assessed by IFA. Indicated values are means (n = 3) ± SEM. Each point represents the mean of one experiment. Three experiments were repeated. *, P < 0.05; **, P < 0.01 (Student's t test). **(I)** Images of IFA of sporozoite in cells stained with YFP (green), UIS4 (red), and DAPI (blue). Bars, 5 µm. Data are representative of three independent experiments. **(J)** Images of IFA of sporozoite in cells stained with anti-UIS3 (green), anti-UIS4 (red), and DAPI (blue). Bars, 5 µm. Data are representative of three independent experiments. N.S., not significant; hpi, hours post-infection.

Given that ionomycin treatment overcomes CXCR4 deficiency for parasite transformation and infection in vitro and that host cell-free sporozoites in Ca^{2+}-containing media show signs of EEFs, sporozoites inoculated in mice might be able to transform into EEFs in the infected hepatocytes if various stimulations elevate the intracellular Ca^{2+} levels in a CXCR4-independent manner. Moreover, CXCR4 inhibition impairs the expression of UIS4, but not UIS3, on the PV membrane after *P. berghei* sporozoite invasion. Given that translation of UIS4 transcripts is repressed at the mosquito stage and released only after host cell invasion (Silvie et al., 2014; Silva et al., 2016), CXCR4–mediated up-regulation of Ca^{2+} in host cells might regulate the release of repressed translation of UIS4 transcripts in sporozoites. Regarding malaria prevention, our study has revealed that CXCR4 blockade inhibits *P. falciparum* sporozoite transformation in hepatocytes (Fig. 4 K). Most antimalaria drugs targeting *Plasmodium*-derived molecules eventually lead to drug resistance in these parasites (Flannery et al., 2013; Antony and Parija, 2016). Despite the risk of side effects or the limited usage during the liver stage of *P. falciparum*, a CXCR4 inhibitor could be used to prophylactically prevent malaria, an approach that could potentially offset the development of drug resistance in this human malaria parasite.

Materials and methods

Mice, cells, parasites, and insects

C57BL/6N mice were obtained from SLC. PKCζ-KO mice were maintained under specific pathogen–free conditions. All animal experiments were conducted with the approval of the Animal Research Committee of Research Institute for Microbial Diseases in Osaka University, Osaka, Japan. Huh7 cells were maintained in RPMI (Nacalai Tesque) containing 10% heat-inactivated FBS, 100 U/ml penicillin, and 0.1 mg/ml streptomycin. HC-04 cells were maintained in DMEM/Ham's F12 media (Invitrogen) containing 10% heat-inactivated FBS, 100 U/ml penicillin, and 0.1 mg/ml streptomycin. To prepare primary hepatocytes, mice were anesthetized and their livers isolated. Primary hepatocytes were prepared using liver digestion medium (Thermo Fisher Scientific). Primary hepatocytes were maintained in Williams' E medium (Life Technologies) containing 1xGlutaMAX-I (Life Technologies), 10% heat-inactivated FBS, 100 U/ml penicillin, 0.1 mg/ml streptomycin, 10 ng/ml EGF (Sigma-Aldrich), 1×GlutaMAX (Thermo Fisher Scientific), 2 mM L-glutamine (Sigma-Aldrich), and 10 mg/ml insulin (Roche). Cryopreserved primary human hepatocytes (HUCPQ) derived from three different individuals were obtained from Lonza. Cells were thawed in Human Thawing Medium (MCHT50P; Lonza). Primary human hepatocytes were maintained in Hepatocyte Maintenance Medium (MM250; Lonza). *P. berghei* ANKA sporozoites and *P. falciparum* NF54 sporozoites were obtained from dissection of the salivary glands of infected *Anopheles stephensi* mosquitoes reared at the Insectary at the Research Institute for Microbial Diseases (Osaka University, Osaka, Japan) or at the Insectary at the Johns Hopkins Malaria Research Institute (Johns Hopkins University, Baltimore, MD), respectively. *P. berghei* and *P. falciparum* sporozoites were isolated into Ca^{2+}- and FBS-free DMEM (21068028; Thermo Fisher Scientific) before use.

Reagents

Antibodies against PKCζ (9372), MET (4560), AKT (9272s), phospho-AKT (9271), ERK1/2 (9102), and phospho-ERK (9101) were obtained from Cell Signaling. CXCR4 (60042–1-Ig), NGFR (55014–1-AP), KRBP (10386–1-AP), SULF2 (12260–1-AP), and dihydrofolate reductase (15194–1-AP) were obtained from Proteintech. Antibodies against CD160 (ab202845), C1orf114 (ab121933), and CTRP4 (ab36871) were obtained from Abcam. Anti-IκBα (sc-371) and NF-κB p65 (sc-8008) were obtained from Santa Cruz. Anti–β-actin antibody (A1978) was obtained from Sigma-Aldrich. Antibodies against *Plasmodium* UIS4 (LS-C204260/53255) and *Plasmodium* HSP70 (LS-C109068/25028) were obtained from LSBio. Anti-*P. falciparum* CSP (MRA-183A) was obtained from MR4. Polyclonal anti-UIS3 was raised in a rabbit against its recombinant protein, which was produced by the pET system (Clontech) in *Escherichia coli*. Anti-AMA1 was kindly provided by Prakash Srinivasan (Johns Hopkins Malaria Research Institute, Baltimore, MD). Recombinant human HGF (100-39) was obtained from Peprotech.

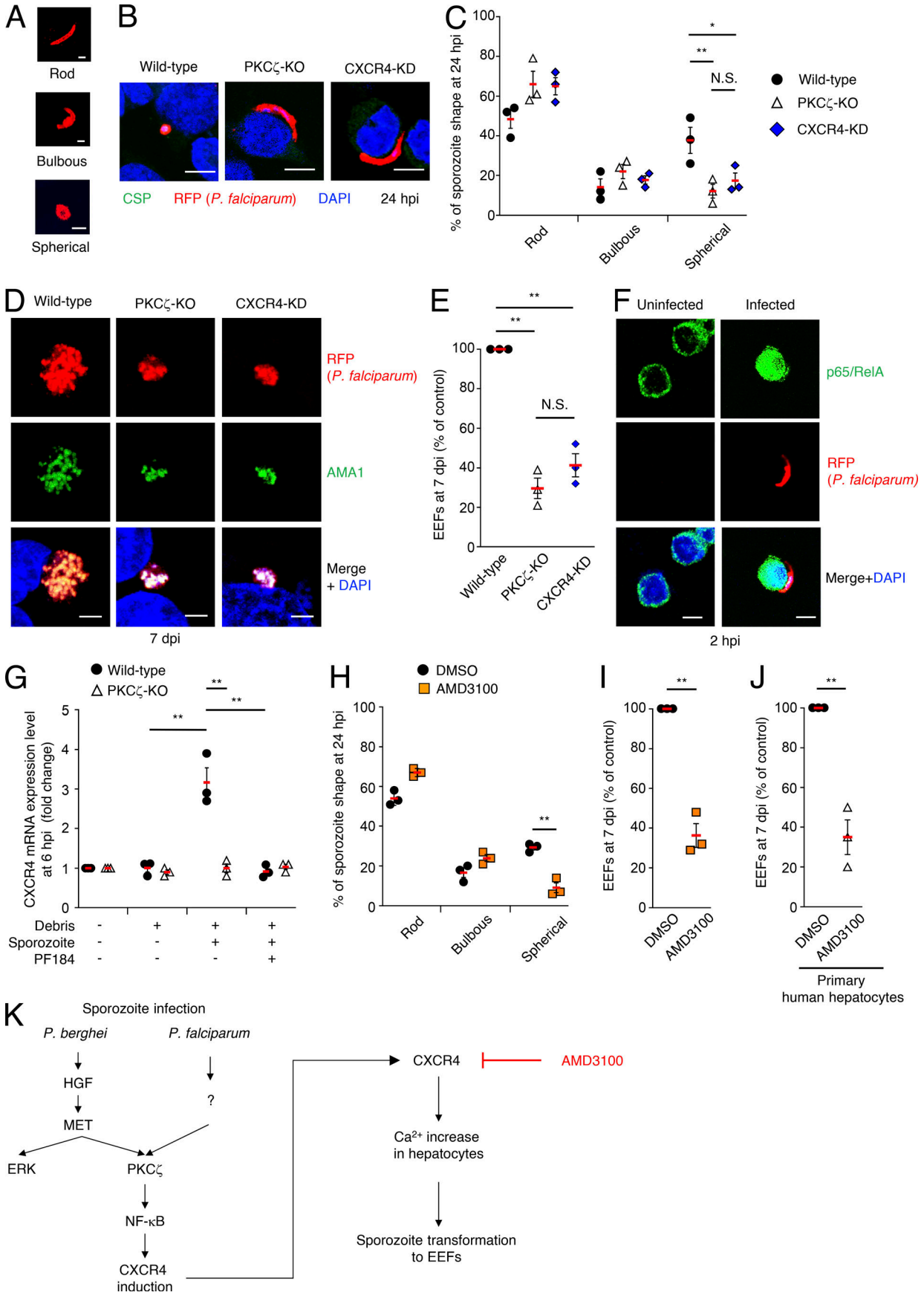

Figure 4. **CXCR4 is required for liver *P. falciparum* development. (A)** Images illustrating *P. falciparum* sporozoite differentiation into EEFs in HC-04 cells. Rod-shaped sporozoites initially acquire a bulbous shape and subsequently become spherical. Bars, 5 µm. **(B–E)** WT, PKCζ-KO, or CXCR4-KD HC-04 cells were infected with *P. falciparum* sporozoites. **(B and C)** Parasite shapes 24 h after sporozoite infection were assessed by IFA. Bars, 5 µm. **(B)** Data are representative of three independent experiments. **(C)** Indicated values are means (n = 3) ± SEM. Each point represents the mean of one experiment. Three experiments were repeated. *, P < 0.05; **, P < 0.01 (Student's t test). **(D and E)** EEFs at 7 d after sporozoite infection were counted using IFA. Bars, 10 µm. **(D)** Data are representative of three independent experiments. **(E)** Indicated values are means (n = 3) of ± SEM. Each point represents the mean of one experiment. Three experiments were repeated. **, P < 0.01 (Student's t test). **(F)** HC-04 cells were uninfected or infected with *P. falciparum* sporozoites. Localization of p65/RelA at 2 h after sporozoite infection was assessed by IFA. Bars, 5 µm. Data are representative of three independent experiments. **(G)** HC-04 cells were treated or not with PF184 (500 nM) for 4 h, as indicated, and then infected or not with *P. falciparum* sporozoites or treated with mosquito debris for 6 h, as indicated. The graphs report the quantitative RT-PCR analysis of CXCR4 mRNA levels. Indicated values are means (n = 3) ± SEM. Each point represents the mean of one experiment. Three experiments were repeated. **, P < 0.01 (Student's t test). **(H and I)** Effect of AMD3100 (1 µM) on *P. falciparum* development in HC-04 cells. **(H)** EEFs at 7 d after sporozoite infection were counted using IFA. Indicated values are means (n = 3) ± SEM. Each point represents the mean of one experiment. Three experiments were repeated. **, P < 0.01 (Student's t test). **(I)** Parasite shapes 24 h after sporozoite infection were assessed by IFA. Indicated values are means (n = 3) ± SEM. Each point represents the mean of one experiment. Three experiments were repeated. **, P < 0.01 (Student's t test). **(J)** Effect of AMD3100 (1 µM) on *P. falciparum* development in human primary hepatocytes. EEFs at 7 d after sporozoite infection were counted using IFA. Indicated values are means (n = 3) ± SEM. Each point represents the mean of one experiment. Three experiments were repeated. **, P < 0.01 (Student's t test). **(K)** Scheme of host signaling pathway for liver stage *P. berghei* or *P. falciparum* transformation. N.S., not significant; dpi, days post-infection; hpi, hours post-infection.

Plasmid construction for the generation of genome-edited human cell lines

All genomic deficient cell lines were generated with the px330 plasmid CRISPR/Cas9 system. The insert fragment of MET, PKCζ, CXCR4, SULF2, ZNF426, C1orf114, C1QTNF4, and CD160 guide RNA (gRNA) were generated by annealing primers. All the primers used in this study are listed in Table S1. These insert fragments were inserted into the BbsI site of the cloning vector containing U6 promoter to generate gRNA expressing plasmids pMET_gRNA1, pMET_gRNA2, pPKCζ_gRNA1, pPKCζ_gRNA2, pCXCR4_gRNA1, pCXCR4_gRNA2, pSULF2_gRNA1, pSULF2_gRNA2, pZNF426_gRNA1, pZNF426_gRNA2, pC1orf114_gRNA1, pC1orf114_gRNA2, pC1QTNF4_gRNA1, pC1QTNF4_gRNA2, pCD160_gRNA1, and pCD160_gRNA2 respectively. The insert fragment was cut out by XhoI and SalI from the pMET_gRNA2, pPKCζ_gRNA2, pCXCR4_gRNA2, pSULF2_gRNA2, pZNF426_gRNA2, pC1orf114_gRNA2, pC1QTNF4_gRNA2, and pCD160_gRNA2 vector and ligated into the XhoI site of the pMET_gRNA1, pPKCζ_gRNA1, pCXCR4_gRNA1, pSULF2_gRNA1, pZNF426_gRNA1, pC1orf114_gRNA1, pC1QTNF4_gRNA1, and pCD160_gRNA1 vector to generate plasmids pMET_gRNA1/2, pPKCζ_gRNA1/2, pCXCR4_gRNA1/2, pSULF2_gRNA1/2, pZNF426_gRNA1/2, pC1orf114_gRNA1/2, pC1QTNF4_gRNA1/2, and pCD160_gRNA1/2. The insert fragment was cut out by KpnI and MluI from pMET_gRNA1/2, pPKCζ_gRNA1/2, pCXCR4_gRNA1/2, pSULF2_gRNA1/2, pZNF426_gRNA1/2, pC1orf114_gRNA1/2, pC1QTNF4_gRNA1/2, and pCD160_gRNA1/2 vector, respectively, and ligated into the KpnI and MluI site of the pEF6-hCas9-Puro vector.

Generation of KD and KO human cell lines by CRISPR/Cas9 genome editing

Human cells were electroporated with the pEF6-hCas9-Puro vector containing target gRNA1/2 using NEPA21 (Nepa Gene). 24 h after electroporation, 2 µg/ml puromycin was added for 7 d to select cells stably harboring genes of interest. To confirm the reduction of target protein expression, CXCR4, SULF2, ZNF426, C1orf114, C1QTNF4, or CD160 protein expression was analyzed by Western blotting. To isolate MET- or PKCζ-deficient single-cell clones, cells were plated in limiting dilution in 96-well plates. To confirm complete target gene deficiency, MET or PKCζ protein expression was analyzed by Western blotting.

Complementation of MET-KO, PKCζ-KO, or CXCR4-KD Huh7 cells

To construct the mammalian expression vectors for complementation of MET, PKCζ, or CXCR4, cDNA fragments were amplified using primer pairs MET_F and MET_R, PKCζ_F and PKCζ_R, or CXCR4_F and CXCR4_R. The primer sequences are listed in Table S1. cDNA fragments encoding each protein were ligated into the pMRX-Puromycin retroviral vector to generate constructs, respectively. The sequences of all of the constructs were confirmed by sequencing analyses with an ABI PRISM Genetic Analyzer 3130xl (PE Applied Biosystems). Plat-E packaging cells were transfected with the retroviral vectors. 48 h after transfection, supernatants containing the retrovirus were collected and filtered to remove the packaging cells. Then, MET-KO, PKCζ-KO, or CXCR4-KD Huh7 cells were incubated with the retrovirus-containing supernatants for 6 h. After removal of the retrovirus, Huh7 cells were incubated for 24 h without puromycin and subsequently incubated for 48–72 h with 2 µg/ml puromycin to select for drug-resistant cells. The expression of MET, PKCζ, and CXCR4 introduced by the retroviral vectors was assessed by Western blot analysis.

Generation of PKCζ-KO mice by CRISPR/Cas9 genome editing

The insert fragments of mouse PKCζ (mPKCζ)_gRNA1 or mPKCζ_gRNA2 was generated using the primers listed in Table S1. The T7-transcribed mPKCζ_gRNA1/2 PCR products were gel purified and used for the subsequent generation of gRNA. MEGAshortscript T7 (Life Technologies) was used for the generation of gRNA. mRNA encoding the RNA-guided DNA endonuclease Cas9 was generated by in vitro transcription using the mMESSAGE mMACHINE T7 ULTRA kit (Life Technologies), and the template was amplified by PCR using pEF6-hCas9-Puro and the primers T7Cas9_IVT_F and Cas9_R and gel purified. The synthesized gRNA and Cas9 mRNA were purified using the MEGAclear kit (Life Technologies) and eluted in RNase-free water (Nacalai Tesque). To obtain PKCζ-KO mice, 6-wk-old female C57BL/6 mice were superovulated and mated to C57BL/6

males. Fertilized one-cell-stage embryos were collected from the oviducts, and the Cas9-encoding mRNA (100 ng/µl) and gRNA (50 ng/µl) were injected into the cytoplasm as described previously (Sasai et al., 2017). The injected live embryos were transferred into the oviducts of pseudopregnant Institute of Cancer Research females at 0.5 d after coitus. Heterozygous mice were intercrossed to generate PKCζ-KO mice for use in the in vivo assays. The PKCζ-KO mice were born at Mendelian ratios and were healthy. The expression of PKCζ proteins in primary hepatocytes was analyzed by Western blotting.

Generation of YFP- and luciferase-expressing *P. berghei*

To express YFP and luciferase in *P. berghei* ANKA, construct encoding YFP and luciferase fusion protein (YFPluc) were cloned into the plasmid vector pSK-1-cssu (Niikura et al., 2013), which contains a selectable marker cassette encoding human dihydrofolate reductase (*hdhfr*) under control of the elongation factor 1 α (*ef-1α*) promoter, a GFP expression cassette under the control of the *P. berghei* heat shock protein 70-1 (*hsp70-1*) promoter, and homology arms of the cssu/dssu ribosomal gene locus of *P. berghei*. pSK-1-cssu was digested with NheI and BglII; therefore, GFP was removed. Subsequently, the YFPluc fragment was cloned into the NheI and BglII site of pSK-1-cssu. To obtain the *P. berghei* YFPluc, transfection was done by electroporation using the Amaxa nucleofector kit. The mutant parasites were selected by pyrimethamine for 2 wk, and then a clonal line expressing YFP and luciferase was obtained by limiting dilution.

Assessment of *P. berghei* or *P. falciparum* numbers in hepatocytes

For in vitro experiments, 2.5×10^5 Huh7 cells were infected with 6×10^4 *P. berghei* YFPluc sporozoites. After 3 h of sporozoite addition to the cells, the *P. berghei* number was counted by staining with anti-UIS3. When parasites were positive for both UIS3 and YFP, we defined them as intracellular parasites (invading parasites). The *P. berghei* number at 24 or 48 h after adding sporozoites in cells was counted by staining with anti-UIS3 or anti-UIS4. Also, we defined parasites stained with both UIS4 and YFP as developed EEFs. Alternatively, the *P. berghei* EEF number 48 h after adding sporozoites was quantified by luciferase intensity.

RFP (TdTomato)-expressing *P. falciparum* sporozoites were used for the assessment of *P. falciparum* EEFs. To count *P. falciparum* EEF numbers, a well (24-well plate) containing 1×10^5 HC-04 cells per well. *P. falciparum* sporozoites (5×10^4) were added to the well at day 0. To assess parasite infection, the *P. falciparum* number was counted after 3 h by staining with anti-CSP. CSP-negative and RFP-positive parasites were considered to be intracellular; CSP-positive and RFP-positive parasites were extracellular or cell traversing. We changed the culture medium daily to prevent bacterial contamination derived from mosquitoes. At day 3 after infection, the HC-04 cells were passaged to two wells to expand the cells. At day 5 after infection, cells were collected from the two wells and the number was counted. Depending on the cell number, the infected HC-04 cells were passaged to several wells containing a coverglass per each well. Cryopreserved primary human hepatocytes were thawed, and the number was counted. Cells were seeded in glass-bottom dishes (1.2×10^5 cells per dish) 1 d before *P. falciparum* sporozoite infection. At day 0, 6×10^4 sporozoites were added to the glass-bottom dishes. The culture medium was routinely changed every day. At day 7 after infection, the infected HC-04 cells or primary human hepatocytes were fixed and stained with anti-CSP and anti–AMA-1 antibodies. Since AMA-1 is a merozoite marker (Vaughan et al., 2012), AMA-1– and RFP-positive parasites were considered to be developed EEFs.

Validation of the EEF number was counted as described previously (Sinnis et al., 2013). Briefly, *P. berghei* EEFs in 50 representative fields per well were counted. For *P. falciparum*, the number of EEFs on all cover glasses was counted.

Measurement of the transformation rates was measured as described previously (Kaiser et al., 2003). Round parasites with no head or tail projections are defined as spherical. Crescent (or banana)-shaped sporozoites are defined as rod. Intermediate forms between rod and spherical parasites are defined as bulbous. Each measurement was performed three biological replicates (three independent experiments) using sporozoites isolated from different cages of mosquitoes.

For in vivo experiments, mice were intravenously infected with 1×10^4 *P. berghei* sporozoites or intraperitoneally infected with 5×10^5 *P. berghei* malaria–parasitized RBCs.

Assessment of parasitemia

Daily thin blood smears were obtained from all infected mice 1 d after infection and stained by Giemsa. Parasitemia was assessed by counting ≥5×10^3 RBCs.

Assessment of vascular leakage

Mice were injected intravenously with 200 µl 2% Evans Blue (Sigma-Aldrich) at 6.5 d after challenge with *P. berghei* sporozoites. Mice were sacrificed 1 h after injection, and brains were isolated and photographed followed by determination of the brain weight. Brains were then placed in 2 ml formamide (Nacalai Tesque) for 48 h at 37°C. The Evans Blue concentration was measured at 620 nm in an ELISA reader using 100 µl of solution. Concentration of Evans Blue was calculated using a standard curve starting at 200 µg/ml. Evans Blue content is expressed as "µg Evans Blue/g brain" in figures.

Measurement of in vivo luciferase activity by an in vivo imaging system

Mice were injected intravenously with 10^5 *P. berghei* YFPluc, and bioluminescence was assessed at 24 or 48 h after infection. For the detection of bioluminescence, mice were intraperitoneally injected with 3 mg d-luciferin (Promega) in 200 µl PBS, maintained for 10 min to allow adequate dissemination of the luciferin, and then anesthetized with isoflurane (Nacalai Tesque). Abdominal photon emission was assessed by in vivo imaging system (IVIS-Spectrum; Xenogen) and analyzed by Living Image software (Xenogen).

Quantitative RT-PCR

Total RNA was extracted, and cDNA was synthesized using Verso Reverse transcription (Thermo Fisher Scientific). Quantitative RT-PCR was performed with a CFX connect real-time

PCR system (Bio-Rad Laboratories) using the Go-Taq Real-Time PCR system (Promega). The values were normalized to the amount of GAPDH for human cells or human DHFR (hDHFR) expressed under the control of EF-1α promoter for *P. berghei* in each sample. The primer sequences are listed in Table S1.

Western blot analysis

Cells or parasites were lysed in lysis buffer (0.5% Nonidet P-40, 150 mM NaCl, and 20 mM Tris-HCl, pH 7.5) containing a protease inhibitor cocktail (Roche) and phosphatase inhibitor cocktail (Nacalai Tesque). Cell lysate proteins were separated by SDS-PAGE and transferred to polyvinylidene difluoride membranes (Immobilon-P; Millipore) and subjected to Western blot analysis using the indicated antibodies.

Measurement of luciferase intensity in vitro

Cells were infected with the *P. berghei* YFPluc, and luciferase activity in cell lysates was measured. To measure the number of parasites, whole cells were collected 48 h after infection and lysed with 100 µl lysis buffer (Promega) and sonicated. After centrifugation at 20,000 ×*g* at 4°C, the luciferase intensity of the supernatant was measured using the Dual Luciferase Reporter Assay System (Promega) and GLOMAX 20/20 luminometer (Promega). The activity percentages of the experimental cells over WT cells are reported as "Luciferase intensity (% of control)" in figures.

Immunofluorescence assay (IFA)

For in vitro cells, Huh7 or HC-04 cells were cultured on glass coverslips or in 8-well chamber slides, infected with *P. berghei* or *P. falciparum* for the indicated times. For liver tissues, livers were taken from mice after 15 h after *P. berghei* sporozoite infection, fixed by 3.7% paraformaldehyde for 2 d, and then replaced by 10% sucrose for 24 h, 20% sucrose for 24 h, and 30% sucrose for 24 h. Samples were embedded in paraffin. 15-µm-thick sections of samples were made with a Cryostat CM1860 (Leica) and air-dried for 24 h. Cell and tissue samples were fixed for 10 min at room temperature in PBS containing 3.7% paraformaldehyde. Cell and tissue samples were permeabilized with PBS containing 0.1% Triton X-100 for 5 min and then blocked with 8% FBS in PBS for 1 h at room temperature. Next, cells were incubated with the indicated primary antibodies for 1 h at 37°C, followed by incubation with Alexa Fluor 488–, Alexa Fluor 594–, or Alexa Fluor 647–conjugated secondary antibodies (Molecular Probes) and DAPI for 1 h at 37°C in the dark. Finally, coverslips were mounted onto glass slides with PermaFluor (Thermo Fisher Scientific) or chamber slides were covered by coverslips. Liver samples were stained with anti-GFP (M048-3; MBL) and DAPI, since *P. berghei* expresses YFP protein. All samples were analyzed using confocal laser microscopy (FV1200 IX-83; Olympus).

Calcium flux assay

Huh7 culture medium was replaced with a Ca^{2+}-containing HBSS buffer. Cells were then incubated with 2 µM Rhod-4 (21120; AAT Bioquest) for 1 h. After incubation, cells were washed twice and resuspended in loading buffer without FBS, stimulated with HGF (50 ng/ml) or infected *P. berghei* sporozoites, and analyzed. Ca^{2+} signals were analyzed using a BZ-X800 All-in-one Fluorescence Microscope (Keyence).

In vitro parasite transformation assay in Huh7 cells treated with ionomycin

Ionomycin (1 µg/ml; Nacalai Tesque) was added to the cell culture medium for 15 min. Cells were then washed three times with PBS and infected with *P. berghei* sporozoites. At the indicated times after infection, parasite shapes or parasite number was assessed by IFA or luciferase assay.

In vitro parasite transformation assay in a host cell–free system

P. berghei sporozoites (1×10^5) were isolated into Ca^{2+}- and FBS-free DMEM (21068028; Thermo Fisher Scientific). *P. berghei* sporozoites were incubated at 37°C for 24 h in FBS-free DMEM with or without 1 mM Ca^{2+} (Calcium Chloride Dihydrate; Nacalai Tesque). Parasite shapes were assessed 24 h after incubation. The expression of HSP70 in parasites was detected by Western blotting. hDHFR expressed under the control of the EF-1α promoter was used as a control. The expression of S-type rRNA in parasites was detected by RT-PCR. Total RNA was extracted using RNeasy Mini kit (QIAGEN), and cDNA was synthesized using Verso reverse transcription (Thermo Fisher Scientific). PCR was performed by using primer pairs Pb-S type_F and Pb-S type_R or Pb-18srRNA_F and Pb-18s rRNA_R. Pb 18s rRNA was used for control. PCR was done for 30 cycles at 95°C for 15 s, 58°C for 30 s, and 72°C for 3 min. The primer sequences are listed in Table S1. Parasite shapes were assessed using confocal laser microscopy.

Treatment of various inhibitors and HGF

For in vitro experiments, AMD3100 (1 µM; Sigma-Aldrich), anti-HGF (20 µg/ml; R&D Systems), PF184 (500 nM; Tocris), or FR182024 (10 µM; Merck Millipore) was added to cell culture media 4 h before infection. Each inhibitor and medium were changed at 0, 4, and 24 h after infection.

For in vivo experiments, AMD3100 (10 mg/kg) was intraperitoneally injected into mice at 24 and 12 h before infection. After intravenous infection of sporozoites, mice were injected with AMD3100 at 0, 12, and 24 h after infection. According to the manufacturer's protocol for AMD3100 (also known as Plerixafor; Genzyme Plerixafor Injection Investigator's Brochure, 2009, version 13, May 27, 2009), a half-life of AMD3100 was previously shown to be ∼5–6 h. Also, the manufacturer reported that the effect of AMD3100 in vivo continues four half-life times (∼20–24 h). In addition, our preliminary experiments to test how often normal mice can be treated with AMD3100 suggested that mice treated with AMD3100 (10 mg/kg) every 6 h become unhealthy. Therefore, we decided to administer AMD3100 treatment in mice every 12 h; treatments were performed at 24 h and 12 h before infection and at 0 h, 12 h, and 24 h after infection.

T cell purification and adoptive cell transfer

T cells were isolated from the spleens of WT or PKCζ-KO mice using the Pan T Cell Isolation Kit II according to the manufacturer's instructions (Miltenyi Biotec). In brief, splenocytes were stained with Pan T Cell Biotin-Antibody Cocktail (Miltenyi Biotec), followed by addition of Pan T Cell Micro Bead Cocktail (Miltenyi Biotec) before separation using a MACS Separator

(Miltenyi Biotec). After sorting, the purity of T cells was assessed by flow cytometry and confirmed to be ∼92–97% (data not shown). The 2 × 10^6 T cells isolated from WT of PKCζ-KO mice were transferred into each PKCζ-KO mouse intravenously. The number of transferred T cells (2 × 10^6 cells) was twice the number (10^6 cells) that had been previously shown to initiate T cell–dependent responses sufficiently in naive C57BL/6 mice (Shaw et al., 2015). 12 h after T cell transfer, mice were intravenously infected with 5 × 10^3 *P. berghei* sporozoites.

RNA-seq analysis

To identify PKCζ-dependent HGF-inducible or *P. berghei* sporozoite-inducible genes, 2.5 × 10^5 WT or PKCζ-KO Huh7 cells were infected or not with 5 × 10^5 *P. berghei* sporozoites, treated or not with HGF. Salivary glands that were isolated from uninfected 50 mosquitoes, washed in PBS, and homogenized in 700 µl Ca^{2+} DMEM are defined as "mosquito debris." Huh7 cells treated with 100 µl mosquito debris were used for further RNA extraction. Total RNA was extracted from whole cells using RNeasy Mini Kit (Qiagen) according to the manufacturer's instructions. Library preparation was performed using a TruSeq stranded mRNA sample prep kit (Illumina) according to the manufacturer's instructions. Whole-transcriptome sequencing was applied to the RNA samples with an Illumina HiSeq 2500 platform in 75-base single-end mode. Illumina Casava version 1.8.2 software was used for base calling. Sequenced reads were mapped to the human reference genome sequences (hg19) using TopHat version 2.0.13 in combination with Bowtie2 version 2.2.3 and SAMtools version 0.1.19. The number of fragments per kilobase of exon per million mapped fragments (FPKM) was calculated using Cuffnorm version 2.2.1. The analysis flow to select PKCζ-dependent genes is described in the Fig. S2 A legend. The accession number for the raw data in this study is available under Gene Expression Omnibus accession no. GSE130442.

Statistical analysis

Each point represents mean (from three technical replicates) of one individual experiment. Therefore, three points in all graphs represent three means derived from three independent experiments (three biological replicates). All statistical analyses were performed using Prism 7 (GraphPad). The statistical significance of differences in mean values was analyzed by using an unpaired two-tailed Student's *t* test. P values <0.05 were considered to be statistically significant. The statistical significance of differences in survival times of mice between two groups was analyzed by Kaplan–Meier survival analysis log-rank test.

Online supplemental material

Fig. S1 shows normal invasion of *P. berghei* sporozoites into anti-HGF–treated WT Huh7 cells and MET-KO or PKCζ-KO Huh7 cells. Fig. S1 also shows that survival rates of PKCζ KO mice infected with *P. berghei* merozoites are normal. Fig. S2 shows full pictures of RNA-seq and comparative analysis between WT and PKCζ-KO Huh7 cells or between control and HGF-treated Huh7 cells. Fig. S3 shows that AMD3100 treatment in WT Huh7 cells and mice phenocopy PKCζ-KO cells and mice in terms of *P. berghei* sporozoite infection, and it also shows that CXCL12 induction in response to *P. falciparum* sporozoite infection in HC-04 cells is dependent on PKCζ and NF-κB. Table S1 lists details of primers used in this study.

Acknowledgments

We thank Mari Enomoto (Osaka University) for secretarial and technical assistance. We also thank Sung-Jae Cha, Patricia Hess Alvarenga, Wei Huang, and Christopher Kizito (Johns Hopkins University) for preparation of *P. falciparum* sporozoites. We thank Shunsuke Yamamoto (Oita Medical University) for helpful discussion.

This work was supported by the Japan Agency for Medical Research and Development Research Program on Emerging and Re-emerging Infectious Diseases (JP18fk0108047), Japanese Initiative for Progress of Research on Infectious Diseases for Global Epidemic (JP18fm0208018), and US–Japan Cooperative Medical Sciences Program Collaborative Awards 2016 (16jk0210010h0001); the Ministry of Education, Culture, Sports, Science and Technology Grant-in-Aid for Scientific Research on Innovative Areas (17K15677 and 19H00970); the Institute for Enzyme Research, Joint Usage/Research Center Cooperative Research Grant; Tokushima University; the Takeda Science Foundation; the Cell Science Research Foundation; the Mochida Memorial Foundation on Medical and Pharmaceutical Research; the Uehara Memorial Foundation; the Naito Foundation; the Astellas Foundation for Research on Metabolic Disorders; and the Research Foundation for Microbial Diseases of Osaka University.

The authors declare no competing financial interests.

Author contributions: H. Bando, M. Jacobs-Lorena, and M. Yamamoto designed research. H. Bando, S. Iwanaga, A. Pradipta, S. Tanaka, A. Soga, S. Fukumoto, and M. Yuda set up the insect facility to obtain *P. berghei* sporozoites and generated transgenic *P. berghei* at Osaka University. H. Bando, Y. Lee, J.S. Ma, N. Sakaguchi, and T. Okamoto performed experiments using *P. berghei* sporozoites. M. Sasai and Y. Matsuura set up administrative experimental protocols for all experiments in this study. D. Okuzaki performed RNA-seq analysis. H. Bando, J. Vega-Rodríguez, and M. Jacobs-Lorena prepared *P. falciparum* sporozoites and performed experiments. H. Bando, Y. Lee, M. Jacobs-Lorena, and M. Yamamoto wrote the manuscript. M. Yamamoto supervised all experiments.

Submitted: 3 December 2018
Revised: 20 March 2019
Accepted: 8 May 2019

References

Amino, R., D. Giovannini, S. Thiberge, P. Gueirard, B. Boisson, J.F. Dubremetz, M.C. Prévost, T. Ishino, M. Yuda, and R. Ménard. 2008. Host cell traversal is important for progression of the malaria parasite through the dermis to the liver. *Cell Host Microbe.* 3:88–96. https://doi.org/10.1016/j.chom.2007.12.007

Antony, H.A., and S.C. Parija. 2016. Antimalarial drug resistance: An overview. *Trop. Parasitol.* 6:30–41. https://doi.org/10.4103/2229-5070.175081

Bladt, F., D. Riethmacher, S. Isenmann, A. Aguzzi, and C. Birchmeier. 1995. Essential role for the c-met receptor in the migration of myogenic

precursor cells into the limb bud. *Nature.* 376:768–771. https://doi.org/10.1038/376768a0

Brochet, M., and O. Billker. 2016. Calcium signalling in malaria parasites. *Mol. Microbiol.* 100:397–408. https://doi.org/10.1111/mmi.13324

Calvo-Calle, J.M., A. Moreno, W.M. Eling, and E.H. Nardin. 1994. In vitro development of infectious liver stages of P. yoelii and P. berghei malaria in human cell lines. *Exp. Parasitol.* 79:362–373. https://doi.org/10.1006/expr.1994.1098

Carrolo, M., S. Giordano, L. Cabrita-Santos, S. Corso, A.M. Vigário, S. Silva, P. Leirião, D. Carapau, R. Armas-Portela, P.M. Comoglio, et al. 2003. Hepatocyte growth factor and its receptor are required for malaria infection. *Nat. Med.* 9:1363–1369. https://doi.org/10.1038/nm947

Cowman, A.F., J. Healer, D. Marapana, and K. Marsh. 2016. Malaria: Biology and Disease. *Cell.* 167:610–624. https://doi.org/10.1016/j.cell.2016.07.055

Diaz-Meco, M.T., and J. Moscat. 2012. The atypical PKCs in inflammation: NF-κB and beyond. *Immunol. Rev.* 246:154–167. https://doi.org/10.1111/j.1600-065X.2012.01093.x

Doi, Y., N. Shinzawa, S. Fukumoto, H. Okano, and H. Kanuka. 2011. Calcium signal regulates temperature-dependent transformation of sporozoites in malaria parasite development. *Exp. Parasitol.* 128:176–180. https://doi.org/10.1016/j.exppara.2011.02.011

Donzella, G.A., D. Schols, S.W. Lin, J.A. Esté, K.A. Nagashima, P.J. Maddon, G.P. Allaway, T.P. Sakmar, G. Henson, E. De Clercq, and J.P. Moore. 1998. AMD3100, a small molecule inhibitor of HIV-1 entry via the CXCR4 co-receptor. *Nat. Med.* 4:72–77. https://doi.org/10.1038/nm0198-072

Flannery, E.L., A.K. Chatterjee, and E.A. Winzeler. 2013. Antimalarial drug discovery - approaches and progress towards new medicines. *Nat. Rev. Microbiol.* 11:849–862. https://doi.org/10.1038/nrmicro3138

Giralt, S., L. Costa, J. Schriber, J. Dipersio, R. Maziarz, J. McCarty, P. Shaughnessy, E. Snyder, W. Bensinger, E. Copelan, et al. 2014. Optimizing autologous stem cell mobilization strategies to improve patient outcomes: consensus guidelines and recommendations. *Biol. Blood Marrow Transplant.* 20:295–308. https://doi.org/10.1016/j.bbmt.2013.10.013

Gomes-Santos, C.S., J. Braks, M. Prudêncio, C. Carret, A.R. Gomes, A. Pain, T. Feltwell, S. Khan, A. Waters, C. Janse, et al. 2011. Transition of Plasmodium sporozoites into liver stage-like forms is regulated by the RNA binding protein Pumilio. *PLoS Pathog.* 7:e1002046. https://doi.org/10.1371/journal.ppat.1002046

Hollingdale, M.R., P. Leland, J.L. Leef, and A.L. Schwartz. 1983. Entry of Plasmodium berghei sporozoites into cultured cells, and their transformation into trophozoites. *Am. J. Trop. Med. Hyg.* 32:685–690. https://doi.org/10.4269/ajtmh.1983.32.685

Huang, S., N. Ouyang, L. Lin, L. Chen, W. Wu, F. Su, Y. Yao, and H. Yao. 2012. HGF-induced PKCζ activation increases functional CXCR4 expression in human breast cancer cells. *PLoS One.* 7:e29124. https://doi.org/10.1371/journal.pone.0029124

Ishino, T., K. Yano, Y. Chinzei, and M. Yuda. 2004. Cell-passage activity is required for the malarial parasite to cross the liver sinusoidal cell layer. *PLoS Biol.* 2:E4. https://doi.org/10.1371/journal.pbio.0020004

Ishino, T., Y. Chinzei, and M. Yuda. 2005. A Plasmodium sporozoite protein with a membrane attack complex domain is required for breaching the liver sinusoidal cell layer prior to hepatocyte infection. *Cell. Microbiol.* 7:199–208. https://doi.org/10.1111/j.1462-5822.2004.00447.x

Kaiser, K., N. Camargo, and S.H. Kappe. 2003. Transformation of sporozoites into early exoerythrocytic malaria parasites does not require host cells. *J. Exp. Med.* 197:1045–1050. https://doi.org/10.1084/jem.20022100

Kaushansky, A., and S.H. Kappe. 2011. The crucial role of hepatocyte growth factor receptor during liver-stage infection is not conserved among Plasmodium species. *Nat. Med.* 17:1180–1181, author reply :1181. https://doi.org/10.1038/nm.2456

Kumar, N., H. Nagasawa, J.B. Sacci Jr., B.J. Sina, M. Aikawa, C. Atkinson, P. Uparanukraw, L.B. Kubiak, A.F. Azad, and M.R. Hollingdale. 1993. Expression of members of the heat-shock protein 70 family in the exoerythrocytic stages of Plasmodium berghei and Plasmodium falciparum. *Parasitol. Res.* 79:109–113. https://doi.org/10.1007/BF00932255

Lee, A.M., B.R. Kanter, D. Wang, J.P. Lim, M.E. Zou, C. Qiu, T. McMahon, J. Dadgar, S.C. Fischbach-Weiss, and R.O. Messing. 2013. Prkcz null mice show normal learning and memory. *Nature.* 493:416–419. https://doi.org/10.1038/nature11803

Leirião, P., S.S. Albuquerque, S. Corso, G.J. van Gemert, R.W. Sauerwein, A. Rodriguez, S. Giordano, and M.M. Mota. 2005. HGF/MET signalling protects Plasmodium-infected host cells from apoptosis. *Cell. Microbiol.* 7:603–609. https://doi.org/10.1111/j.1462-5822.2004.00490.x

Littman, D.R. 1998. Chemokine receptors: keys to AIDS pathogenesis? *Cell.* 93:677–680. https://doi.org/10.1016/S0092-8674(00)81429-4

Martin, P., R. Villares, S. Rodriguez-Mascarenhas, A. Zaballos, M. Leitges, J. Kovac, I. Sizing, P. Rennert, G. Márquez, C. Martínez-A, et al. 2005. Control of T helper 2 cell function and allergic airway inflammation by PKCzeta. *Proc. Natl. Acad. Sci. USA.* 102:9866–9871. https://doi.org/10.1073/pnas.0501202102

Meis, J.F., J.P. Verhave, P.H. Jap, R.E. Sinden, and J.H. Meuwissen. 1983. Malaria parasites--discovery of the early liver form. *Nature.* 302:424–426. https://doi.org/10.1038/302424a0

Meis, J.F., J.P. Verhave, P.H. Jap, and J.H. Meuwissen. 1985. Transformation of sporozoites of Plasmodium berghei into exoerythrocytic forms in the liver of its mammalian host. *Cell Tissue Res.* 241:353–360. https://doi.org/10.1007/BF00217180

Mellado, M., J.M. Rodríguez-Frade, S. Mañes, and C. Martínez-A. 2001. Chemokine signaling and functional responses: the role of receptor dimerization and TK pathway activation. *Annu. Rev. Immunol.* 19:397–421. https://doi.org/10.1146/annurev.immunol.19.1.397

Ménard, R., V. Heussler, M. Yuda, and V. Nussenzweig. 2008. Plasmodium pre-erythrocytic stages: what's new? *Trends Parasitol.* 24:564–569. https://doi.org/10.1016/j.pt.2008.08.009

Mikolajczak, S.A., V. Jacobs-Lorena, D.C. MacKellar, N. Camargo, and S.H. Kappe. 2007. L-FABP is a critical host factor for successful malaria liver stage development. *Int. J. Parasitol.* 37:483–489. https://doi.org/10.1016/j.ijpara.2007.01.002

Mota, M.M., G. Pradel, J.P. Vanderberg, J.C. Hafalla, U. Frevert, R.S. Nussenzweig, V. Nussenzweig, and A. Rodríguez. 2001. Migration of Plasmodium sporozoites through cells before infection. *Science.* 291:141–144. https://doi.org/10.1126/science.291.5501.141

Mueller, A.K., N. Camargo, K. Kaiser, C. Andorfer, U. Frevert, K. Matuschewski, and S.H. Kappe. 2005a. Plasmodium liver stage developmental arrest by depletion of a protein at the parasite-host interface. *Proc. Natl. Acad. Sci. USA.* 102:3022–3027. https://doi.org/10.1073/pnas.0408442102

Mueller, A.K., M. Labaied, S.H. Kappe, and K. Matuschewski. 2005b. Genetically modified Plasmodium parasites as a protective experimental malaria vaccine. *Nature.* 433:164–167. https://doi.org/10.1038/nature03188

Naldini, L., E. Vigna, R.P. Narsimhan, G. Gaudino, R. Zarnegar, G.K. Michalopoulos, and P.M. Comoglio. 1991. Hepatocyte growth factor (HGF) stimulates the tyrosine kinase activity of the receptor encoded by the proto-oncogene c-MET. *Oncogene.* 6:501–504.

Niikura, M., S. Inoue, S. Mineo, Y. Yamada, I. Kaneko, S. Iwanaga, M. Yuda, and F. Kobayashi. 2013. Experimental cerebral malaria is suppressed by disruption of nucleoside transporter 1 but not purine nucleoside phosphorylase. *Biochem. Biophys. Res. Commun.* 432:504–508. https://doi.org/10.1016/j.bbrc.2013.02.004

Prudêncio, M., A. Rodriguez, and M.M. Mota. 2006. The silent path to thousands of merozoites: the Plasmodium liver stage. *Nat. Rev. Microbiol.* 4:849–856. https://doi.org/10.1038/nrmicro1529

Prudêncio, M., C.D. Rodrigues, M. Hannus, C. Martin, E. Real, L.A. Gonçalves, C. Carret, R. Dorkin, I. Röhl, K. Jahn-Hoffmann, et al. 2008. Kinome-wide RNAi screen implicates at least 5 host hepatocyte kinases in Plasmodium sporozoite infection. *PLoS Pathog.* 4:e1000201. https://doi.org/10.1371/journal.ppat.1000201

Sasai, M., N. Sakaguchi, J.S. Ma, S. Nakamura, T. Kawabata, H. Bando, Y. Lee, T. Saitoh, S. Akira, A. Iwasaki, et al. 2017. Essential role for GABARAP autophagy proteins in interferon-inducible GTPase-mediated host defense. *Nat. Immunol.* 18:899–910. https://doi.org/10.1038/ni.3767

Sattabongkot, J., N. Yimamnuaychoke, S. Leelaudomlipi, M. Rasameesoraj, R. Jenwithisuk, R.E. Coleman, R. Udomsangpetch, L. Cui, and T.G. Brewer. 2006. Establishment of a human hepatocyte line that supports in vitro development of the exo-erythrocytic stages of the malaria parasites Plasmodium falciparum and P. vivax. *Am. J. Trop. Med. Hyg.* 74:708–715. https://doi.org/10.4269/ajtmh.2006.74.708

Schmidt, C., F. Bladt, S. Goedecke, V. Brinkmann, W. Zschiesche, M. Sharpe, E. Gherardi, and C. Birchmeier. 1995. Scatter factor/hepatocyte growth factor is essential for liver development. *Nature.* 373:699–702. https://doi.org/10.1038/373699a0

Shaw, T.N., P.J. Stewart-Hutchinson, P. Strangward, D.B. Dandamudi, J.A. Coles, A. Villegas-Mendez, J. Gallego-Delgado, N. van Rooijen, E. Zindy, A. Rodriguez, et al. 2015. Perivascular Arrest of CD8+ T Cells Is a Signature of Experimental Cerebral Malaria. *PLoS Pathog.* 11:e1005210. https://doi.org/10.1371/journal.ppat.1005210

Shortt, H.E., and P.C. Garnham. 1948. Pre-erythrocytic stage in mammalian malaria parasites. *Nature.* 161:126. https://doi.org/10.1038/161126a0

Silva, P.A., A. Guerreiro, J.M. Santos, J.A. Braks, C.J. Janse, and G.R. Mair. 2016. Translational Control of UIS4 Protein of the Host-Parasite Interface Is Mediated by the RNA Binding Protein Puf2 in Plasmodium berghei Sporozoites. *PLoS One.* 11:e0147940. https://doi.org/10.1371/journal.pone.0147940

Silvie, O., S. Briquet, K. Müller, G. Manzoni, and K. Matuschewski. 2014. Post-transcriptional silencing of UIS4 in Plasmodium berghei sporozoites is important for host switch. *Mol. Microbiol.* 91:1200–1213. https://doi.org/10.1111/mmi.12528

Sinnis, P., P. De La Vega, A. Coppi, U. Krzych, and M.M. Mota. 2013. Quantification of sporozoite invasion, migration, and development by microscopy and flow cytometry. *Methods Mol. Biol.* 923:385–400. https://doi.org/10.1007/978-1-62703-026-7_27

Tachibana, K., S. Hirota, H. Iizasa, H. Yoshida, K. Kawabata, Y. Kataoka, Y. Kitamura, K. Matsushima, N. Yoshida, S. Nishikawa, et al. 1998. The chemokine receptor CXCR4 is essential for vascularization of the gastrointestinal tract. *Nature.* 393:591–594. https://doi.org/10.1038/31261

Tavares, J., P. Formaglio, S. Thiberge, E. Mordelet, N. Van Rooijen, A. Medvinsky, R. Ménard, and R. Amino. 2013. Role of host cell traversal by the malaria sporozoite during liver infection. *J. Exp. Med.* 210:905–915. https://doi.org/10.1084/jem.20121130

Tsuji, M., D. Mattei, R.S. Nussenzweig, D. Eichinger, and F. Zavala. 1994. Demonstration of heat-shock protein 70 in the sporozoite stage of malaria parasites. *Parasitol. Res.* 80:16–21. https://doi.org/10.1007/BF00932618

Uehara, Y., O. Minowa, C. Mori, K. Shiota, J. Kuno, T. Noda, and N. Kitamura. 1995. Placental defect and embryonic lethality in mice lacking hepatocyte growth factor/scatter factor. *Nature.* 373:702–705. https://doi.org/10.1038/373702a0

Vaughan, A.M., S.A. Mikolajczak, E.M. Wilson, M. Grompe, A. Kaushansky, N. Camargo, J. Bial, A. Ploss, and S.H. Kappe. 2012. Complete Plasmodium falciparum liver-stage development in liver-chimeric mice. *J. Clin. Invest.* 122:3618–3628. https://doi.org/10.1172/JCI62684